Emittance Measurements of a Laser-Wakefield-Accelerated Electron Beam

S. Fritzler,[1] E. Lefebvre,[2] V. Malka,[1] F. Burgy,[1] A. E. Dangor,[3] K. Krushelnick,[3] S. P. D. Mangles,[3] Z. Najmudin,[3] J.-P. Rousseau,[1] and B. Walton[3]

[1]*Laboratoire d'Optique Appliquée–ENSTA, UMR 7639, CNRS, École Polytechnique, 91761 Palaiseau, France*
[2]*Département de Physique Théorique et Appliquée, CEA/DAM Ile-de-France, BP 12, 91680 Bruyères-le-Châtel, France*
[3]*Blackett Laboratory, Imperial College of Science, Technology, and Medicine, London SW7 2BZ, United Kingdom*

(Received 6 November 2003; published 23 April 2004)

The transverse emittance of a relativistic electron beam generated by the interaction of a high-intensity laser with an underdense plasma has been measured with the "pepper-pot" method. For parameters pertaining to the forced laser wakefield regime, we have measured an emittance as low as $(2.7 \pm 0.9)\,\pi$ mm mrad for (55 ± 2) MeV electrons. These measurements are consistent with 3D particle-in-cell simulations of the experiment, which additionally show the existence of a relatively large halo around the beam core.

DOI: 10.1103/PhysRevLett.92.165006 PACS numbers: 52.38.Kd, 29.27.Fh, 41.75.Lx

The interaction of high-intensity laser pulses with plasmas has received great attention due to the very large electric [1] and magnetic [2] fields that can be generated during these interactions. These fields can have amplitudes greater than several hundreds of GV/m [3] and MG [2], respectively. Such electric field amplitudes are several orders of magnitude greater than those currently attainable with conventional accelerator technology. Hence laser plasma interactions promise to play a role in future generations of particle accelerators. Interestingly, laser generated plasmas are capable of directly accelerating background particles and have been demonstrated to be efficient sources of bright, energetic, and collimated electron [3], proton [4], as well as γ-ray [5] beams. To further assess the potential of laser wakefields as a next-generation acceleration technique, a better characterization of such accelerated beams is necessary. The emittance, in particular, is a measure deduced from the beam distribution in phase space that quantifies its divergence and focusability. Hence it is an important figure of merit for any source of energetic particles, and the emittance of laser accelerated electrons must be investigated.

For efficient electron acceleration, the laser pulse must interact with an underdense plasma, where the initial electron density, n_e, is below the critical density, n_c, so enabling the laser beam to propagate in the medium. In the self-modulated laser wakefield regime and for laser powers, P_L, in excess of the critical power for relativistic self-focusing, $P_c \approx 1.7 \times 10^{-2}\, n_c/n_e$ (TW), the mutual enhancement of the laser envelope modulation and electron plasma wave growth [6] can lead to breaking of the plasma wave and strong electron acceleration. A maximum electron energy of 100 MeV was reported in an experiment using a 25 J, 1 ps, 1 μm laser focused into a plasma at $n_e = 1.5 \times 10^{19}$ cm^{-3} [7]. Measurements of the angular distribution of such electron beams by nuclear activation techniques indicated that they are well centered on the laser propagation axis. The full width at half maximum (FWHM) opening cone of electrons above 11 MeV was found to change between 8° and 12° for various plasma densities [8].

Recently, a substantial improvement in the quality as well as maximum energy of laser generated electron beams was reported in the forced laser wakefield (FLWF) regime, where the laser pulse duration is about the inverse plasma period, $\tau_L \sim 2\pi\omega_p^{-1}$ [9]. In this regime, a nonlinear wakefield is driven above wave breaking by the intense ultrashort laser beam. Because of its strong ponderomotive force the front of the laser pulse pushes electrons forward while its rear propagates in the density depression of the relativistic plasma wave. Therefore the head of the laser pulse has a lower group velocity than the tail, which leads to compression. This enhances the growth of the wakefield, driving it to wave breaking in just one plasma wave cycle. The angular divergence of the accelerated electrons was shown for 35-plus MeV electrons to have a FWHM of less than 5°. It has been conjectured that this suggests that the energetic electrons in the beam have a very low emittance [10].

In this Letter we present the first experimental emittance measurements of an electron beam produced by a laser plasma accelerator. We also present full 3D simulations of the beam acceleration and transport. We show that high-energy electrons generated in the FLWF regime have a normalized vertical emittance which is comparable to modern electron accelerators. The simulations are consistent with the experimental results, and in addition suggest that the collimated beam core is surrounded by a halo, that can include up to 40% of the particle number at high energy.

The experiment was performed on the Ti:sapphire "salle jaune" laser at Laboratoire d'Optique Appliquée, which operates in chirped-pulse amplification mode at a wavelength, λ_L, of 820 nm [11]. The laser delivered 30 fs FWHM linearly polarized pulses with on target energies of 1 J. The laser beam was focused with an $f/18$ off-axis

parabolic mirror onto a sharp-edged, constant density profile, 3 mm diameter supersonic helium gas jet, which provided an initial plasma electron density, n_e, of 2.5×10^{19} cm^{-3}. The waist of the focal spot was 18 μm, resulting in vacuum focused intensities of the order of 3×10^{18} W/cm^2, which corresponds to a normalized laser vector potential, $a_0 = eA/m_e c^2$, of 1.2. The spectrum of the electron beam was measured with a tunable dispersing magnetic field and five biased silicon surface barrier detectors giving the on-axis electron beam distribution shown in Fig. 1. The total charge of the electron beam was measured using an integrating current transformer and found to be about 5 nC.

The emittance of an electron beam is usually given for a finite, narrow, electron energy interval. Yet as can be seen in Fig. 1 the energy spectrum of the electron beam generated in the FLWF is broad. Hence accurate emittance measurement in this case requires that the electron energies are dispersed. This was achieved with a secondary magnet directly installed behind the gas jet nozzle. Electrons entered this compact magnet of 5 cm diameter through a 50 msr stainless steel collimator, which served to obtain a reasonable energy resolution while retaining the opening cone of the electron beam. As this setup dispersed electrons in the horizontal plane of the experiment, we could only measure the transverse emittance of the electron beam out of this plane, i.e., along the x axis, orthogonal to the direction of laser propagation and its polarization.

The normalized rms emittance is defined as the root means square (rms) correlation between the space, x, and reduced momentum, x', coordinates of all beam electrons in the (x, x') 2D phase space

$$\epsilon^n_{x,\mathrm{rms}} = \beta\gamma\sqrt{\langle x^2\rangle\langle (x')^2\rangle - \langle xx'\rangle^2}, \qquad (1)$$

where β and γ are the usual relativistic factors, and $x' = p_x/p_z$ is the electron angle with respect to the laser axis, which is also the overall beam direction. Graphically, the (x, x') phase space plot is a measure of the electron beam divergence as a function of position across the beam. In addition to the definition given above, one can also define the normalized effective emittance, ϵ^n_x, as the surface encompassed by the beam in the (x, x') space [12]. For an elliptical shape and uniform beam density in (x, x'), the two measures of emittance are linked by $\epsilon^n_x = 4\epsilon^n_{x,\mathrm{RMS}}$. The "pepper-pot" method [13] that we used to measure emittance is closely related to this second definition of emittance, as it involves measuring the spread of the electron beam divergence, $\triangle x'$, at various positions across its diameter. Area and shape of the beam in phase space is then deduced from position and intensity distribution of the beam spots on the RCF. To this end, most of the electron beam is blocked by a "pepper-pot" mask that allows electrons only at selected position to pass through, as illustrated in Fig. 2. The lead mask was fixed behind the magnet in a region where its field has decayed to a negligible amplitude. Its thickness was varied between 2 and 6 mm depending on the electron energy. It is punctured by (750 ± 100) μm diameter holes. The mask is displaced vertically along the x axis with a 5 μm precision stepping motor, scanning the entire vertical diameter of the electron beam. 150 laser shots were accumulated at each "pepper-pot" mask position. Since the electron beam can move on a shot to shot basis, these experimental emittance values can be considered as an upper value of the real one.

The electron beamlet passing through these holes was visualized at various distances behind the mask with radiochromic film (RCF), which has a spatial resolution below 10 μm [14] and which was scanned with the same resolution directly after the experiment. To avoid direct illumination of the RCF by the laser beam, the film was shielded with aluminum foil. Scattering of electrons within these thin foils of 25 μm thickness has been corrected for. Measuring the distances indicated in Fig. 2, one can calculate the spread of the angular divergence in a straightforward manner to be

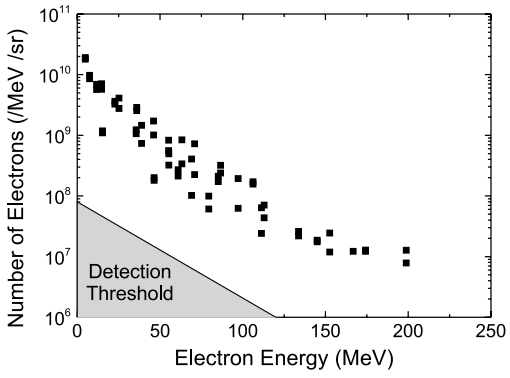

FIG. 1. Electron spectrum for $n_e = 2.5 \times 10^{19}$ cm^{-3} and a laser intensity of 3.0×10^{18} W/cm^2.

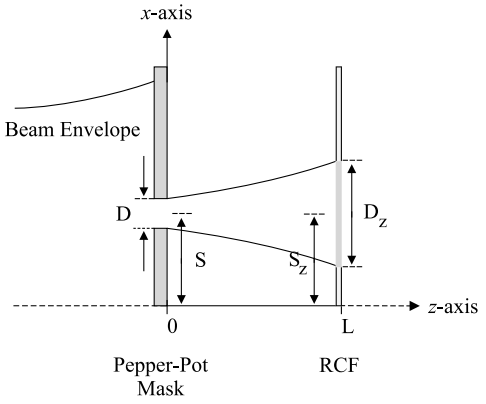

FIG. 2 (color online). Cross section of a beamlet passing through a pinhole of the "pepper-pot" mask. D_z is measured as the e^{-1} width of the RCF spots.

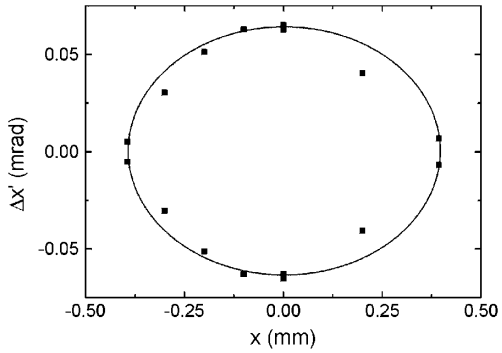

FIG. 3. Two-dimensional $\triangle x'(x)$ phase-space distribution for an electron energy of (55 ± 2) MeV. The dots represent the maximum extent of the beam. The solid line is a fit for the phase space ellipse.

$$\triangle x' = L^{-1}\left(D_z - D\frac{S_z}{S}\right), \tag{2}$$

which is deduced from the ballistic spread of the electron beamlets during their propagation from the pepper-pot mask to the RCF. The normalized vertical beam emittance, ϵ_x^n, in (π mm mrad), is obtained as π^{-1} times the phase space area encompassed by this curve, $\triangle x'(x)$.

A plot of $\triangle x'$ for (55 ± 2) MeV electrons across the entire vertical electron beam diameter is given in Fig. 3, from which ϵ_x^n was deduced to be (2.7 ± 0.9) π mm mrad. This value is indeed comparable with the performance of modern accelerators [15]. As can be seen in Fig. 4, ϵ_x^n decreased in this regime as a function of electron energy.

The experiment was modeled numerically with the 3D particle-in-cell code CALDER. A "moving window" capability was used to follow the laser pulse as it propagates through the plasma. The laser pulse was input as Gaussian in time and space with a FWHM of 30 fs and 18 μm, respectively. The normalized laser vector potential was $a_0 = 1.3$, corresponding to a laser irradiance of 3.5×10^{18} W/cm^2 for $\lambda_L = 820$ nm. The plasma electron density in the simulation was $0.02n_c$, i.e., 3.3×10^{19} cm^{-3} for a 820 nm laser wavelength. A volume of $65 \times 27 \times 54$ μm^3 of plasma, comoving with the laser pulse, was modeled with 8.7×10^8 macroelectrons in a 2.2×10^8 cell mesh. Ions were treated as a fixed neutralizing background. Because of computing time constraints, the plasma length was limited to 790 μm, which is consistent with the calculations reported in [9].

The transverse emittance in the simulation was measured at different times during the beam propagation and after its exit from the plasma, in the four energy intervals that were used in the experiment. The effect of a 50 msr collimator was accounted for by excluding all particles with an angle to the propagation axis larger than 7.2°. Phase space projections in the (x, x') plane are then constructed, from which the effective emittance, ϵ_x^n, can be calculated. Figure 5 represents one such plot, obtained shortly after the beam exit from plasma at 818 μm, for (55 ± 2) MeV electrons. A feature of the wakefield-produced beam is its relatively large halo, which is apparent as the light blue cloud surrounding the beam core. As a result the emittance is dependent on the beam fraction over which it is calculated [12]. For instance, the dashed black ellipse in Fig. 5 corresponds to an emittance of 5.1 π mm mrad and encompasses 70% of the electrons. To better quantify this effect, we determined a minimum emittance curve by finding the largest beam fraction encompassed by ellipses of given areas, centered on $(x = 0, x' = 0)$. The resulting curves, for the four relevant energy intervals, are plotted in Fig. 6 together with the measured emittance values. We observe that the experimental points for the three lowest energies are consistent with the simulations if 10% to 15% of the beam electrons are in the halo and escape detection in the experiment. The 55 MeV measurement is consistent with a larger halo of 40% of the beam.

Ideally, and in the calculations, the emittance reflects the distribution of all electrons in phase space. However, single electrons cannot be measured with the RCF, due to its limited sensitometric response [16]. For each energy bin it is thus interesting to compare the detected electron number, which can be deduced from the optical density of

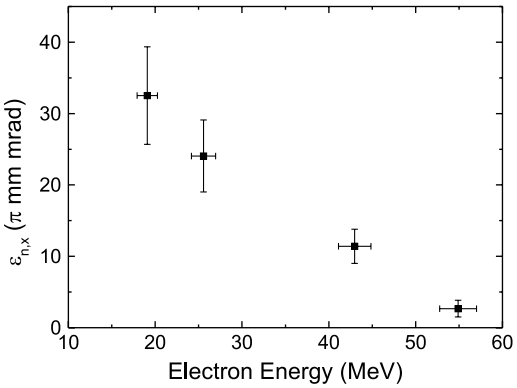

FIG. 4. Normalized vertical emittance ϵ_x^n as a function of electron energy.

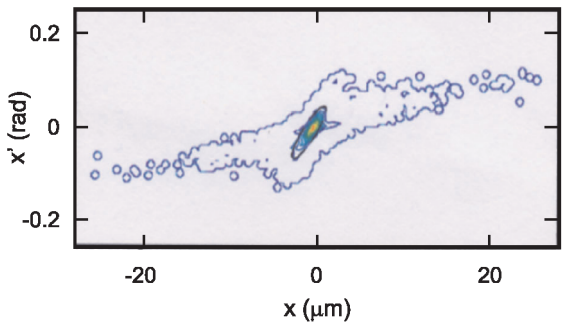

FIG. 5 (color online). Phase-space projections in the (x, x') plane for (55 ± 2) MeV electrons. The light blue cloud surrounding the electron beam core corresponds to the halo of the beam.

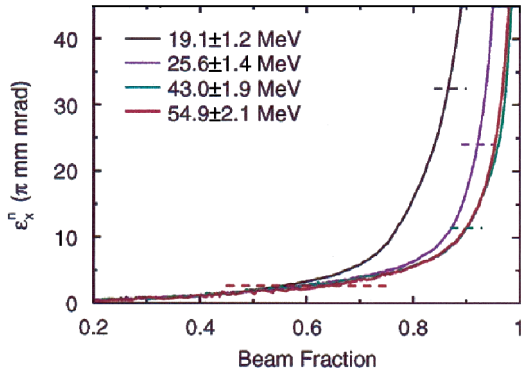

FIG. 6 (color online). Minimum emittance curves as a function of beam fraction derived from the simulation (solid lines), and experimental values (dashed lines). This comparison supports an experimentally undetected beam halo of between 10% and 40% of the total electron number.

the scanned RCF, with the total number of electrons within this bin, as measured with the magnetic spectrometer. This determines the fraction of beam electrons that actually participates in the emittance measurement, and reflects the importance of the electron beam halo. It is found that the calculated experimental ratios are consistent with the beam fractions derived from the simulations, and show the same trend of a larger halo at higher electron energy.

The shape of the high-density region of the phase space, around $(x = 0, x' = 0)$, suggests that the beam core is actually composed of electrons trapped around the axis, inside the fields of the plasma bubble created by the laser pulse [9,17], which perform small-angle transverse oscillations as they propagate. This interpretation is confirmed by the trajectories of test-particles sampling the high-energy electron beam, which show most particles performing small-amplitude oscillations along the laser axis, and occasionally some electrons accelerated out of the main bunch. These free-streaming particles will add up during propagation to constitute the beam halo.

The consistency observed between experiment and simulations gives confidence in the ability of 3D simulations to predict electron source characteristics produced by these sources. Indeed simulations show that modest progress in laser parameters will result in significantly improved source performances. We compute that the interaction of a 10^{20} W/cm^2, 6 μm focal spot, 15 fs duration laser pulse with a 0.01 n_c plasma can lead after 600 μm of propagation to electrons accelerated up to 200 MeV with a very flat distribution and a 22% laser-to-electron energy efficiency, a tenfold increase over the computed efficiency of our present source. After only 300 μm propagation, the effective emittance for (55 ± 2) MeV electrons is almost identical to that calculated for our current source, but with an electron charge, 40 pC, which is more than tripled at this energy. Because of the very flat electron spectrum, a significant number of particles can still be found at higher energy, e.g., the (100 ± 2) MeV electrons form a 22 pC bunch with an effective emittance of 2.5 π mm mrad for the 60% central fraction of the bunch. Thus these measurements are of importance for schemes which envision relativistic laser plasma interactions as a booster for future linear accelerators [17,18].

This work was partially supported by the EU Access to Research Infrastructure under LOA Contract No. HPRI-1999-CT-00086.

[1] T. Tajima and J. Dawson, Phys. Rev. Lett. **43**, 267 (1979); E. Esarey *et al.*, IEEE Trans. Plasma Sci. **24**, 252 (1996).
[2] M. Tatarakis *et al.*, Nature (London) **415**, 280 (2002).
[3] A. Modena *et al.*, Nature (London) **377**, 606 (1995).
[4] E. L. Clark *et al.*, Phys. Rev. Lett. **85**, 1654 (2000); S. P. Hatchett *et al.*, Phys. Plasmas **7**, 2076 (2000).
[5] M. H. Key *et al.*, Phys. Plasmas **5**, 1966 (1998); P. A. Norreys *et al.*, Phys. Plasmas **6**, 2150 (1999).
[6] W. B. Mori, IEEE J. Quantum Electron. **33**, 1 (1997).
[7] D. Gordon *et al.*, Phys. Rev. Lett. **80**, 2133 (1998).
[8] M. I. K. Santala *et al.*, Phys. Rev. Lett. **86**, 1227 (2001).
[9] V. Malka *et al.*, Science **298**, 1596 (2002); Z. Najmudin *et al.*, Phys. Plasmas **10**, 2071 (2003).
[10] K.-C. Tzeng *et al.*, Phys. Plasmas **5**, 2105 (1999).
[11] M. Pittman *et al.*, Appl. Phys. B **74**, 529 (2002).
[12] M. Reiser, *Theory and Design of Charged Particle Beams* (J. Wiley & Sons, New York, 1994).
[13] Y. Yamazaki *et al.*, Nucl. Instrum. Methods Phys. Res., Sect. A **322**, 139 (1992).
[14] W. L. McLaughlin *et al.*, Nucl. Instrum. Methods Phys. Res., Sect. A **302**, 165 (1991).
[15] J. P. Carneiro *et al.*, FERMILAB-Conf-99/271, 1999.
[16] Nuclear Associates, product description, 2002.
[17] A. Pukhov and J. Meyer-ter-Vehn, Appl. Phys. B **74**, 355 (2002).
[18] S. Fritzler *et al.*, Appl. Phys. Lett. **83**, 3888 (2003).